Positive Pion Photoproduction from Hydrogen for Incident Photon Energies 300–750 MeV

C. BETOURNE, J. C. BIZOT, J. PEREZ-Y-JORBA, AND D. TREILLE
Ecole Normale Supérieure, Laboratoire de l'Accélérateur Lineaire, 91-Orsay, France

AND

W. SCHMIDT*
Stanford Linear Accelerator Center, Stanford University, Stanford, California

(Received 8 March 1968)

The differential cross section for the reaction $\gamma+p\rightarrow\pi^+n$ was measured at 19 photon energies between 300 and 750 MeV in the laboratory frame, for pion angles between 0° and 130° in the c.m. system. The pions were analyzed in angle and momentum with a magnetic spectrometer and detected by a counter telescope. The 0° measurements could be achieved, in spite of the excessive positron rate, owing to a mass-spectrometer arrangement. No direct indication for the electromagnetic excitation of the P_{11} resonance (1466 MeV) was found. Comparison is made with theoretical calculations of π^+ photoproduction.

I. INTRODUCTION

MANY detailed and complete angular distributions of single π^+ photoproduction on protons are now available, up to a photon energy $k=1270$ MeV and recent measurements at DESY and SLAC have extended the data even up to 16 GeV.[1,2] In spite of the many data it was not possible to extend phenomenological analyses[3,4] in the region of the D_{13} pion nucleon resonance ($k_R\approx770$ MeV) to lower energies $k<550$ MeV since the information was too scanty. But such an extension of the analyses is necessary in order to see if the results are consistent with the results of the dispersion theory at lower energies around the P_{33} resonance. Such a check could remove at least part of the arbitrariness in formulating a phenomenological model at these higher energies.

The results, which we present in this paper for laboratory photon energies 300–750 MeV, serve three purposes:

First, the new data supply small-angle cross sections which are lacking between the highest measurement of Knapp *et al.*[5] at 290 MeV and the lowest measurement of Beneventano *et al.*[6] at 550 MeV. These cross sections provide a sensitive test for theoretical predictions near 0°, where the results of the different theories usually disagree.

Second, the results allow us to study systematically the effects of the P_{11} resonance (1466 MeV) between the P_{33}(1236 MeV) and D_{13}(1525 MeV) resonances, where the data have been scanty up to now.[7–10]

Third, we undertook to provide data with a better accuracy in order to resolve discrepancies between various experimental results and to allow for a refinement of phenomenological predictions.

II. GENERAL FEATURES OF EXPERIMENTAL METHOD

π^+ mesons are photoproduced by a bremsstrahlung beam incident on a liquid target. They are analyzed by a magnetic spectrometer at momentum p and laboratory angle θ.

The kinematics of the reaction is described in Fig. 1, where k is the laboratory energy of the photon. The

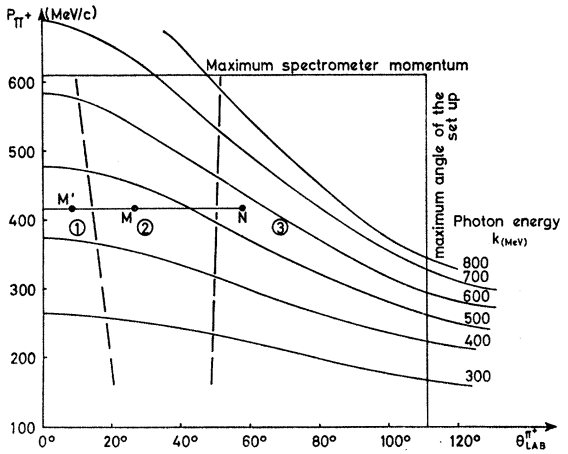

FIG. 1. Kinematics of the three experimental regions.

* On leave of absence from Institut für Experimentelle Kernphysik, Kernforschungszentrum, Karlsruhe, Germany.

[1] S. D. Ecklund and R. L. Walker, Phys. Rev. **159**, 1195 (1967).

[2] H. A. Thiessen, Phys. Rev. **155**, 1488 (1967); G. Buschhorn *et al.*, Phys. Rev. Letters **17**, 1027 (1966); **18**, 571 (1967); A. M. Boyarski *et al.*, *ibid.* **20**, 300 (1968).

[3] G. Schwiderski, thesis, Karlsruhe, 1967 (unpublished); G. Schwiderski and W. Schmidt, Kernforschungszentrum, Karlsruhe Report No. 3/67-1, 1967 (unpublished).

[4] Y. C. Chau, R. G. Moorhouse, and N. Dombey, Phys. Rev. **163**, 1632 (1967).

[5] E. A. Knapp, R. W. Kenney, and V. Perez-Mendez, Phys. Rev. **114**, 605 (1959).

[6] M. Benevantano, R. Finzi, L. Mezzetti, L. Paoluzi, and S. Tazzari, Nuovo Cimento **28**, 1464 (1963).

[7] A. V. Tollestrup, J. C. Keck, and R. M. Worlock, Phys. Rev. **99**, 220 (1955).

[8] M. Heinberg, W. M. Mc Clelland, F. Turkot, W. M. Woodward, R. R. Wilson, and D. M. Zipoy, Phys. Rev. **110**, 1211 (1958).

[9] R. L. Walker, J. G. Teasdale, V. Z. Peterson, and J. I. Vette, Phys. Rev. **99**, 210 (1955).

[10] J. C. Bizot, J. Perez-Y-Jorba, and D. Treille, in *Proceedings of the International Symposium on Electron and Photon Interactions* (Deutsche Physikalische Gesellschaft, Hamburg, 1965), Vol. II.

energy E of the machine is chosen so that k belongs to the flat region of the bremsstrahlung energy curve; but E is below threshold for double photoproduction processes giving a π^+ or μ^+ at the analyzed momentum. Tests of consistency of our energy calibrations were obtained by drawing excitation curves at fixed p and θ and variable E (Fig. 2).

In addition to π^+, other particles are analyzed and reach the detectors. These are essentially protons from π^0 photoproduction and, at forward angles, positrons from electromagnetic pairs. We have, in Fig. 1, distinguished three regions that we now define. n_{e^+}, n_p, and n_{π^+} represent the yield of analyzed electrons, protons, and pions.

$$\textit{Region 1: } n_{e^+} > n_p > n_{\pi^+}.$$
$$\textit{Region 2: } n_p > n_{\pi^+} > n_{e^+}.$$
$$\textit{Region 3: } n_{\pi^+} \geqslant n_p > n_{e^+} \approx 0.01 n_{\pi^+}.$$

In region 3, the small constant rate of e^+ comes from π^0 decay. In region 1, the rate of e^+ increases very rapidly at small angles, and at 0°, even in the most favorable experimental conditions, the ratio n_{e^+}/n_{π^+} is as high as $\sim 10^4$–10^5. Besides e^+ and p, some muons from π^+ decay reach also the detection system.

The two leading factors governing possibilities of discrimination at detection are the following:

(a) Because of the poor duty cycle of the linear accelerator (5×10^{-5}), one must limit the total counting rates to less than 30–40 counts/sec to avoid large and poorly known dead-time losses in the electronics. This sets a lower limit to the time needed for registering a given number of π^+ and the presence of additional background increases this limit.

(b) The limited possibilities of discrimination of the detection system, which will be described in Sec. IV, obviously lead to a possibility of confusion between particles when the rate of background particles is high.

A very conservative rule was applied: When, after momentum analysis, the ratio of the number of background particles over n_{π^+} is equal to or larger than unity, one eliminates (totally or partially) the spurious particles in an appropriate way before detection. So, in region 1, both e^+ and protons are eliminated; in region 2, only protons. The case of μ^+, which we could neither eliminate nor discriminate in the whole range of our measurements, has been treated by computation, the result of the computations being checked by a separate experiment. As a consequence, the experimental procedure is different in each region, as will be seen later. The overlap of two different procedures, near the border of two domains, provides very useful tests of reliability.

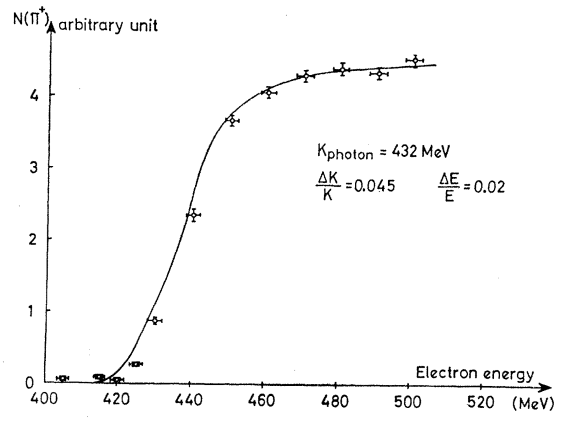

FIG. 2. Pion yield as a function of the electron energy (p and θ fixed).

The elimination of background before detection is a source of π^+ loss through strong interactions and multiple scattering. So, except in region 3, one does not immediately obtain the real number of analyzed π. But the π loss, for a given experimental setup and especially for a given analyzed momentum p, is independent of the angle θ. Therefore, everything being left unchanged except θ (and E), one goes from the measurement point M (or M') (Fig. 1) to some "normalization" point N belonging to region 3. The ratio of π rates in M (or M') and N is, up to kinematical factors, equal to the ratio of the corresponding photoproduction cross sections and since the absolute cross section can be determined in N, we thus get the absolute one in M or M'. Hence the measurement is direct in region 3 and indirect in regions 1 and 2.

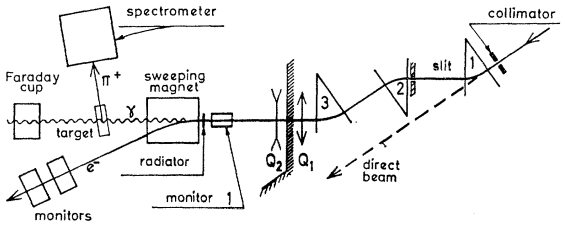

FIG. 3. Experimental layout.

III. EXPERIMENTAL ARRANGEMENT

The electron beam is extracted from the linear accelerator by an achromatic, afocal system composed of three magnets (Fig. 3). A slit before magnet 2 reduces the beam energy resolution to the desired value ($\Delta E/E = 2\%$ in our case). The average energy E is measured with a proton resonance probe. Two quadrupoles Q_1 and Q_2 focus the beam onto the target. A secondary electron emission monitor, of thickness 2×10^{-4} radiation length and stability better than 0.5%, is used to measure the intensity of the electron beam. It is calibrated against a Faraday cup, which is removed from the beam during data taking to reduce background.

The proton beam is produced in a radiator after

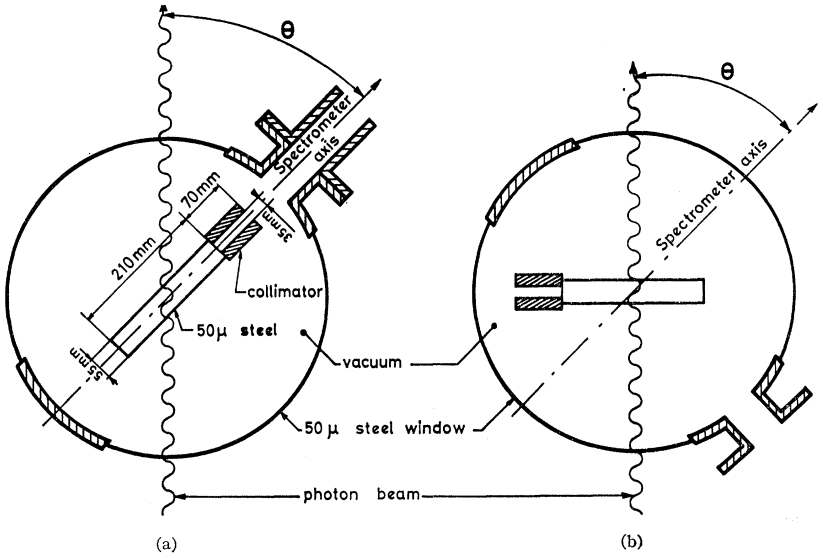

FIG. 4. Target setup.

which the charged particles are swept out by a magnet; the radiator thickness is computed to avoid any further collimation of the bremsstrahlung beam. Foils of copper or aluminum from 0.5–4% radiation length were used as radiators. The photon spectrum was computed with a thick-target bremsstrahlung program[11] which takes into account the electron energy degradation in the radiator and pair production by the photons.

The liquid hydrogen is contained in a target cell (Fig. 4) (55×210 mm, 60 mm height) with 50-μ steel windows, which is directly connected to a 10-liter liquid-hydrogen reservoir, both being enclosed in a vacuum chamber.

In region 3 this vacuum chamber is connected to the spectrometer and can rotate with it [Fig. 4(a)]. The major axis of the target and the optical axis of the spectrometer coincide. A tungsten collimator set parallel to this axis with good accuracy prevents the spectrometer from seeing the target windows and thus eliminates the empty-target background. It also reduces the transverse target width to 35 mm as seen by the spectrometer, so that the useful interaction length of the beam is $35/\sin\theta$ (mm). The electron energy E was always chosen to avoid any contamination from energetic π^+ mesons produced at the tip of the bremsstrahlung spectrum which loses energy in the collimator.

In regions 1 and 2 the target vacuum chamber is independent of the spectrometer. The target is roughly normal to the beam [Fig. 4(b)] and the empty-target background has to be subtracted. In these regions, because of the normalization process used, one need not know the exact target length. (See Sec. V B.)

The magnetic spectrometer[12] (Fig. 5) is made of three deflecting magnets which are electrically set in series. The whole system is symmetric relative to the bisector plane R of magnet 2.

In first-order optics, this spectrometer is triple focusing and its magnification is 1.

In the radial plane: (a) There exists in plane R an intermediate image: All trajectories of the same momentum p_0 and coming from a point O are focused there in a point C, whatever be their emission angle in the radial plane. (b) The radial abscissa in plane R for a trajectory of momentum p depends on the relative difference $(p-p_0)/p_0$ between p and the central momentum p_0. Therefore, one can determine the momentum resolution $\Delta p/p_0$ by a radial slit in plane R. $\Delta p/p_0$ was $\pm 2\%$ in this experiment.

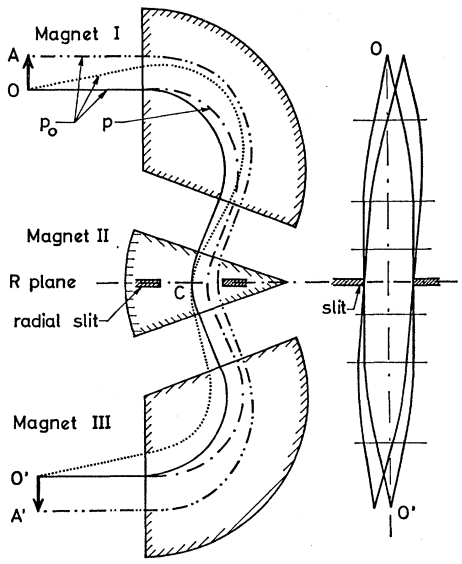

FIG. 5. Optics of the triple focusing spectrometer (sketch).

[11] R. A. Alvarez, Stanford University Laboratory Report No. HEPL 228, 1961 (unpublished).
[12] B. Milman, l'Onde Elec. 42, 310 (1962).

In the transverse plane: (a) The trajectories are independent of momentum. (b) The transverse abscissa in plane R depends only on the transverse angle at emission. (c) A suitable transverse slit in plane R can be used to make the solid angle constant for all points of the target, whatever their distance to the optical axis of the spectrometer.

These optical properties, especially the existence of a radial intermediate image in plane R, allow for another use of this apparatus, in a mass-spectrometer way, as we shall see in Sec. IV.

The spectrometer calibration was performed with the floating-wire technique to an accuracy of 0.5%. The maximum momentum that one can reach is limited to 600 MeV/c by magnet saturation.

In regions 2 and 3 the solid angle was defined by the spectrometer optics itself and not by some entrance slits. It was measured at several momenta using the known e^-p elastic scattering cross section (see Sec. V A). The angular resolution was $\pm 0.8°$ lab in the transverse plane and $\pm 5°$ lab in the radial one, except for the measurements of region 1 where this last value was lowered to $\pm 2°$ lab.

IV. PARTICLE SEPARATION AND IDENTIFICATION OF PIONS

As we explained previously, the structure of the detection system depends on the region explored:

Region 3: The telescope is made of three plastic scintillators designed so as to collect all particles analyzed by the spectrometer. On each counter a bias separates low signals due to the majority of the π^+ from larger signals due to the protons and to about 10% of the π^+ belonging to the tail of the ionization loss spectrum. Proton signals are high in all three counters, while there is no correlation between the value of a π signal from one scintillator to another. Therefore, such a bias eliminates all the protons losing less than one out of a thousand pions.

On the other hand, this telescope does not permit the separation of the muons from the π mesons. This μ contamination must be computed and the calculation will be described in Sec. V.

Region 2: Protons, being here more numerous than pions, are stopped before detection in a carbon absorber set just in front of the telescope. The π loss in the absorber is taken into account as described before, in going from point M to point N. It can reach 60%, when the π momentum corresponds to the first resonance πN. A gas Čerenkov detector rejects the positrons; the pions are detected as before with three plastic scintillators.

Region 1: The rate of the positrons is very important. One cannot eliminate them by means of an absorber in front of the counters. Indeed, it is well known that positrons in matter develop showers and, even after several radiation lengths, e^+ and e^- of small energy may still be present.

On the other hand, pions lose only a small fraction of their momentum by ionization. Such a difference of behavior suggests the possibility of a magnetic separation between the pions and the showers' components, the majority of which have momenta much smaller than the pion momenta.

This separation was achieved with the previously described spectrometer used in a different way (Fig. 6). It was magnetically separated into two parts; the first two magnets compose one side, the third magnet the other side. A lead radiator of 1–6 radiation lengths was set near plane R.

The first part analyzes the particles according to their momentum around p_0. In the radiator they undergo the previously described processes. Then, the second part analyzes the particles according to their loss of momentum in the radiator as seen below. If the second part is set to the average momentum p_π of the π^+ coming out from the absorber, the mesons thus reach the counters, while nearly all components of the showers are swept out.

Because of the existence of an intermediate image in plane R, the total spectrometer is still focusing in energy and in radial angle, in spite of multiple scattering in the radiator, but only for particles losing the same momentum δp in this radiator. Correspondingly, a difference of momentum loss in the radiator is changed into spatial dispersion in the image plane.

One must now distinguish two resolutions: a resolution in analyzed momentum $\Delta p/p_0$, determined as previously by radial slits, and a resolution in momentum loss δp in the radiator determined by the radial size of

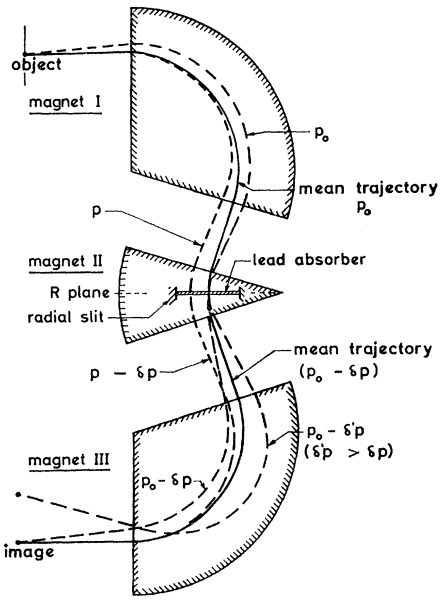

FIG. 6. Optics of the mass spectrometer (sketch).

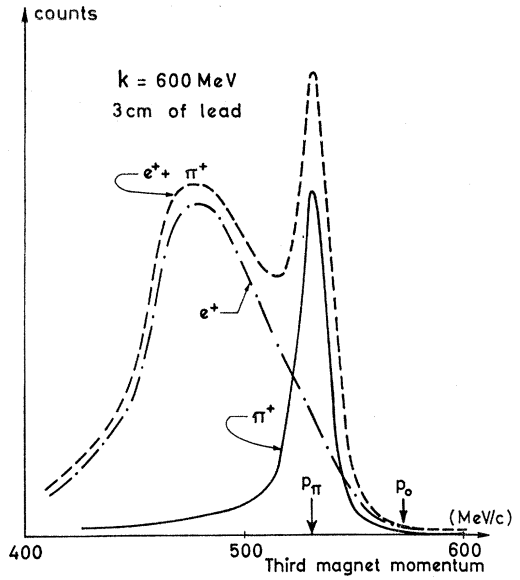

FIG. 7. Separation of positrons from pions with the mass spectrometer.

the counters in image plane. These two functions of the spectrometer are completely independent.

In the transverse plane, because of multiple scattering, the spectrometer is no longer focusing. The resulting loss of π's can reach up to 90%. The previously described normalization procedure accounts perfectly for this loss. Note that the loss of π through strong interactions in the lead radiator is less than 20%. The effect of a transverse slit is the same as before.

Figure 7 shows the e^+ and π^+ spectra as a function of momentum in the third magnet. The ratio n_{e^+}/n_{π^+} at the pion peak still varies 0.5–10 at 0°. One needs an additional rejection at detection. This was achieved by using a gas Čerenkov counter working with Freon 13 under 12 bar, of efficiency 0.997 ± 0.003 to e^+. The uncertainty (0.003) on this efficiency makes 0° measurements below 300 MeV imprecise because the ratio n_{e^+}/n_{π^+} increases very rapidly there.

Electronics: Discriminators and coincidence units are standard Chronetics circuits running on 50 MHz (~15-nsec coincidence resolution). The counts are recorded on 100-MHz scalers, which can register up to four events within the accelerator pulse (~1 μsec).

V. DATA REDUCTION

We shall consider separately the direct measurements of region 3 and the indirect ones of regions 1 and 2. To determine the absolute cross section, one must know the detection solid angle and apply several corrections. On the other hand, the indirect measurements essentially give a ratio between two cross sections; the corrections can be ignored if they are the same at measurement and normalization points. This is almost correct since they depend mostly on the π momentum, which is identical at both points. In the same way, the solid angle completely disappears from the ratio.

A. Absolute Measurements

1. Solid-Angle Determination

The solid angle was determined by measuring, with the same experimental setup, e^-p elastic scattering at several momenta of the final electrons and for low transfers, where the proton form factors are known with great accuracy; the photoproduction spectrum is rather flat on the spectrometer momentum acceptance (curve a of Fig. 8) while an elastic peak intrinsic width (curve b) is much smaller than this 4% acceptance. Thus, to take into account the variation of solid angle with momentum inside this acceptance (curve c), we folded the elastic peak distribution curve with the momentum acceptance by moving the spectrometer central energy q around the fixed energy p_0 of the maximum of the elastic peak. We then obtained curve d by dividing the folding by the acceptance ($0.04\ q$). From the area S under curve d we get the solid angle of the apparatus integrated over the target length L and the spectrometer momentum acceptance $A=\Delta p/p_0$ around momentum p_0:

$$\bar{\Omega}=\frac{1}{AL}\int\int\Omega dA dL \qquad (1)$$

through the relation

$$S=(d\sigma_R/d\Omega)C(\Delta)\bar{\Omega}F. \qquad (2)$$

Here F is the product of the number of incident electrons by the density of target protons per cm^2. $d\sigma_R/d\Omega$ is the Rosenbluth cross section. $C(\Delta)$ is a correction factor due to the fact that the tail of curve d is truncated at $p_0-\Delta$. A good approximation to $C(\Delta)$, if Δ is sufficiently large (fairly larger than the half-width of curve d), is to take the usual form for a normal nonfolded elastic peak.[13] But this correction is valid only for $\Delta/p_0\ll1$, while, as

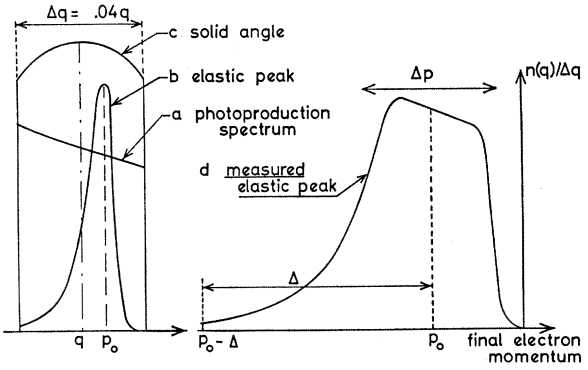

FIG. 8. Normalization process.

[13] L. N. Hand, Phys. Rev. 129, 1834 (1963).

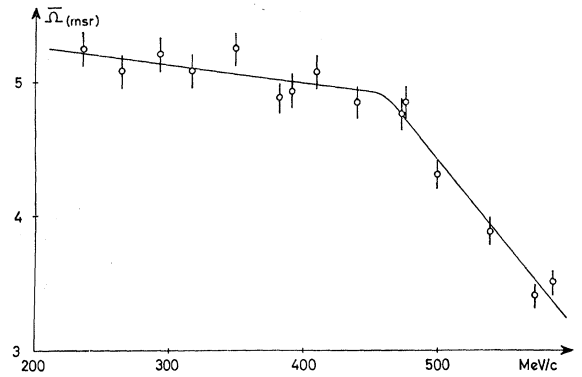

FIG. 9. Mean solid angle of the spectrometer as a function of momentum (note the vertical scale).

we said, we deal with rather high values of Δ. Therefore, we performed slight modifications on $C(\Delta)$ to take into account the fact that, when Δ is large, scattering after radiation and scattering before radiation, leading to the same final energy, occur in fact at different energies. We find that for a given momentum, the value obtained for $\bar{\Omega}$ was constant within 1% when Δ/p_0 was varied rom 3 to 15%. Figure 9 shows the variation of $\bar{\Omega}$ as a unction of momentum. The error on $\bar{\Omega}$ is estimated to 2.5%. The increase of slope at about 450 MeV/c is due to magnet saturation.

2. Corrections

Along the distance from the target to the counters (10 m), a large fraction of the pions decay with emission of a muon in a very small forward cone, at the lowest momentum about 60% of the pion decay.

The counting rate is corrected for the π exponential decrease and for μ^+ contamination since the μ^+ is indistinguishable from the π^+ at detection. The formulation of the μ contamination problem was treated through a Monte Carlo method with the following random variables: (a) the π momentum and direction at emission, (b) its length of flight, according to an exponential law, and (c) the μ emission angles (determining its momentum).

The trajectories in the spectrometer were computed to first order. The calculated μ^+ contamination varies from 12 to 6% of the number of detected π^+ and is thought to be accurate to 2% of this number. These computations were checked at low momentum by actually detecting muons with a water Čerenkov counter. The agreement is satisfactory.

Before leaving the target, the pions traverse 10 cm of hydrogen. Because of the very small angular acceptance of the spectrometer, a pion which undergoes a strong interaction is lost; this effect can reach 10% on the first πN resonance. On the other hand, some π, which initially do not satisfy requirements to be analyzed, may scatter on a proton and subsequently fulfill these requirements; this correction never exceeds 2%.

Electromagnetic effects in the target are twofold: (a) Positive and negative contributions due to multiple scattering cancel one another. (b) The momentum loss by ionization, especially at low energies, changes with momentum inside the accepted band; therefore there may be a 3% difference between the acceptance as being determined by radial slits and its effective value when π are produced. This effect has been accounted for.

In the telescope, similar phenomena occur, the result of which is a decrease of the counting efficiency. By strong interactions in the two first counters, pions are lost; this loss, being a linear function of the thickness of these two counters, has been measured by varying artifically their thickness using additional absorbers of the same material. Multiple scattering has a very small effect and was neglected. The counting rates have been corrected for accidental coincidences and electronic losses which are mainly due to the discriminator dead time.

3. Cross-Section Computation

Once the correct pion rate N_π has been obtained, the cross section in the laboratory system is extracted from the formula

$$N_\pi = N_\gamma n_p (d\sigma/d\Omega)(k,\theta)\bar{\Omega}(p_0), \tag{3}$$

where the photon number N_γ is given by

$$N_\gamma = N_e \rho(k)\Delta k. \tag{4}$$

Here N_e is the electron number, $\rho(k)$ is the bremsstrahlung spectrum density per electron, Δk is the photon energy resolution$=[\partial k/\partial p\ (p_0,\theta)]\Delta p$, and n_p is the proton density per cm^2 along the beam direction. The photon energy resolution Δk is large at high energies and backward angles; therefore, the cross sections have been corrected accordingly.

B. Indirect Measurements

In regions 1 and 2, where the target is transverse, we must perform an empty-target subtraction; this was 20% at 0° and low energies.

The small-angle cross section is obtained from a normalization procedure at an angle α and same momentum p, where the absolute cross section is known by direct measurement; the ratio of cross sections and the ratio of counting rates at θ^0 and α^0 are related simply by

$$\frac{N_\pi(\theta)}{N_\pi(\alpha)} = \frac{(d\sigma/d\Omega)(k(\theta),\theta)N_\gamma(\theta)}{(d\sigma/d\Omega)(k(\alpha),\alpha)N_\gamma(\alpha)}. \tag{5}$$

For each measurement at small angles we have chosen at least two normalization points corresponding to two different angles α. The cross sections at these angles α were computed by interpolation between the absolute results of region 3. As expected, we obtained the same

value for the small-angle cross sections, within statistics, independent of the angle α.

In going from θ to α the effective target length L seen by the spectrometer changes as shown in Fig. 4(b). But as already noted, a transverse slit in the symmetry plane of the spectrometer has been designed to make the acceptance constant for all points of interaction in the target, up to the largest angle α used for normalization. This has been checked experimentally. Therefore the parameter L has no influence on the counting rates. We have also checked that the choice of the resolution in loss of momentum δp does not modify our results.

In the determination of the cross-section ratio all the previously described corrections (π decay, μ correction, π losses, etc.) cancel to first order and only their small differences between 0 and α have to be accounted for.

VI. RESULTS

Table I gives the differential cross sections in the c.m. system, as a function of the pion c.m. angle θ^* for 19 values of the laboratory photon energy. (The 300 and 310 MeV are considered as a single energy.) The result quoted is often the weighted mean of several measurements. The random errors listed represent the statistical error added quadratically to the errors on the dead-time correction and on the secondary electron monitor efficiency. For the indirect measurements, it also includes the normalization uncertainty ($\sim 3\%$). Below 600 MeV, the total cross sections were obtained from least-squares fits of our data, the weight of the backward angles which are missing in our data being negligible. Above 600 MeV, Moravcsik fits were used for the forward angles which are lacking in our data, the contribution of these points being also very weak.

The pion angle θ is known to about 3 min. The corresponding resolution is $\Delta\theta = 0.8°$ lab; the azimuthal resolution $\Delta\phi = \pm 5°/\sin\theta$ lab does not affect the results in regions 2 and 3; in region 1 the angular resolution was always smaller than $\pm 2°$ lab and the quoted results have not been unfolded from this resolution. The fit of the data with a Moravcsik curve shows a negligible influence of this resolution. It is believed that this effect is appreciably smaller than the other experimental errors.

The photon energy calibration is consistent from point to point to about 0.1% and the absolute calibration error is less than 0.5%. The energy resolution depends on the pion momentum and angle and is essentially defined by the spectrometer momentum resolution (4%).

The systematic errors are listed in Table II. The cross sections are plotted on Figs. 10 and 11 to allow for a direct comparison with previous data.[1,2,6–9,14–20] Figure 12 shows excitation curves for fixed values of θ^*.

VII. DISCUSSION OF RESULTS

Below $k = 500$ MeV the new results of this experiment can be compared to absolute predictions following from a new evaluation of fixed-t dispersion relations.[21,22] Above $k = 500$ MeV only phenomenological approaches exist so far.[3,4] The work in Ref. 3 is an extension of the dispersion model at low energies,[21] and we shall base our discussion mainly on those results.

A. General Review

It has been discussed in Ref. 23 that at present our incomplete knowledge of high-energy contributions in dispersion intergrals leaves arbitrary certain contributions to the multipoles $M_{1+}^{3/2}$ and $E_{1+}^{3/2}$ [24] of the first resonance, which vary slowly with energy. As a consequence one is only able to predict the large $M_{1+}^{3/2}$ at resonance within 5–10% and one cannot predict the sign of the small quantity $E_{1+}^{3/2}$ from theory alone. But once $M_{1+}^{3/2}$ $(k=k_R)$ and $E_{1+}^{3/2}$ $(k=k_R)$ are fixed, the energy dependence within the region of the first resonance can safely be predicted for these partial amplitudes. Therefore an effort was made in Ref. 21 to narrow the limits for the parameters $M_{1+}^{3/2}(k_R)$ and $E_{1+}^{3/2}(k_R)$ by fitting certain experimental quantities, which depend sensitively on these parameters. In this way the uncertainty with respect to $E_{1+}^{3/2}(k_R)$ could be reduced considerably and the limits for $M_{1+}^{3/2}(k_R)$ could be made smaller than 5%. The experimental results used were mainly obtained with plane-polarized γ's in π^0 photoproduction. Therefore the dispersion-theory results for π^+ photoproduction presented here in Figs. 10–12 are a prediction (the results correspond to the best solution in Ref. 21).

One observes in Figs. 10–12 a reasonably good agreement. Around the first resonance the largest discrepancies appear near $\theta^* = 90°$, where the theory predicts differential cross sections which are too large. If the parameters chosen to fix $M_{1+}^{3/2}$ and $E_{1+}^{3/2}$ are correct, then one would clearly see here the influence of errors in the small multipoles which should be enhanced around the resonance. The differences between theory and experiment are never larger than those expected (see, e.g., the errors on the theoretical predictions calculated in Ref. 22).

[14] F. P. Dixon and R. L. Walker, Phys. Rev. Letters **1**, 458 (1958). See also revised data in J. H. Boyden, Ph.D. thesis, California Institute of Technology, 1961 (unpublished).

[15] D. Freytag, W. J. Schwille, and R. J. Wedemeyer, Z. Physik **186**, 1 (1965); C. Freitag, D. Freytag, K. Lübelsmeyer, and W. Paul, *ibid.* **175**, 1 (1963).

[16] K. Althoff, H. Fischer, and W. Paul, Z. Physik **175**, 19 (1963).

[17] A. J. Lazarus, W. K. H. Panofsky, and F. R. Tangherlini, Phys. Rev. **113**, 1330 (1959).

[18] R. A. Alvarez, Phys. Rev. **142**, 957 (1966).

[19] L. Hand and C. Schaerf, Phys. Rev. Letters **6**, 229 (1961).

[20] C. Schaerf, Nuovo Cimento **44**, 504 (1966).

[21] J. Engels, A. Müllensiefen, and W. Schmidt, Stanford Linear Accelerator Center Laboratory Report No. SLAC-PUB-415 (unpublished). See also W. Schmidt, Z. Physik **182**, 76 (1964).

[22] F. A. Berends, A. Donnachie, and D. L. Weaver, Nucl. Phys. **B4**, 1 (1967); **B4**, 55 (1967).

[23] J. Engels and W. Schmidt, Phys. Rev. **169**, 1296 (1968).

[24] We use standard notations in pion photoproduction; see, e.g., G. F. Chew, M. L. Goldenberger, F. E. Low, and Y. Nambu, Phys. Rev. **106**, 1345 (1957) or Ref. 21.

TABLE I. Differential cross sections in the c.m. system (μb/sr) and associated standard deviation errors Δ (μb/sr). The π^+ c.m. angle is θ^* (degrees), the laboratory photon energy k (MeV). The total cross section σ_T is in μb.

θ^*	σ	Δ
$k=300$		
0.	8.1	1.4
2.7	8.2	0.8
4.	8.4	0.5
6.7	8.3	0.5
10.	8.3	0.5
13.3	8.3	0.5
$k=310$	$\sigma_T=223$	
50	14.71	0.41
60	16.78	0.47
70	19.13	0.54
80	21.08	0.59
90	21.09	0.59
100	20.77	0.57
110	20.35	0.57
120	20.33	0.57
$k=325$	$\sigma_T=212$	
0.	14.2	0.7
2.7	14.9	0.8
50	15.93	0.46
60	17.23	0.50
70	18.33	0.53
80	19.56	0.57
90	19.62	0.58
100	19.36	0.58
110	18.88	0.58
120	18.08	0.56
$k=350$	$\sigma_T=180$	
0.	18.4	0.8
2.	17.8	0.9
2.7	18.4	0.8
5.	18.7	1.3
7.5	16.7	1.2
10.	17.5	1.3
15.	14.9	1.0
50	15.07	0.43
60	16.17	0.46
70	16.20	0.46
80	16.81	0.48
90	16.62	0.48
100	14.84	0.44
110	14.48	0.44
120	13.61	0.41
130	13.37	0.41
$k=375$	$\sigma_T=141$	
0.	20.0	0.7
50	12.46	0.34
60	13.77	0.38
70	13.16	0.37
80	12.82	0.37
90	12.01	0.35
100	11.44	0.33
110	10.70	0.31
120	10.03	0.30
130	10.18	0.31
$k=400$	$\sigma_T=117$	
0.	18.7	0.9
2.5	19.5	0.7
4.6	18.5	0.7
7.	18.6	0.7
10.	16.4	0.8
14.5	15.5	0.6
21.	13.4	0.5
32.	12.9	0.6
50	11.41	0.31
60	11.33	0.31

θ^*	σ	Δ
$k=400$	$\sigma_T=177$	
70	11.11	0.31
80	10.37	0.29
90	9.42	0.27
100	8.62	0.25
110	8.00	0.23
120	7.12	0.21
130	6.80	0.23
$k=425$	$\sigma_T=97$	
0.	20.6	0.7
60	9.75	0.26
70	9.04	0.24
80	8.85	0.24
90	7.95	0.22
100	6.84	0.19
110	6.43	0.18
120	5.35	0.16
130	5.55	0.16
$k=450$	$\sigma_T=88$	
0.	19.4	0.8
2.9	18.4	0.8
4.3	17.9	0.7
7.2	16.8	0.7
10.8	15.3	0.6
13.5	14.2	0.5
21.	11.1	0.5
30	10.34	0.27
40	9.42	0.25
50	9.72	0.25
60	9.14	0.24
70	8.78	0.23
80	7.91	0.21
90	7.07	0.19
100	6.25	0.18
110	5.57	0.16
120	4.55	0.13
130	4.40	0.13
$k=475$	$\sigma_T=85$	
0.	18.8	0.8
30	10.42	0.27
40	9.64	0.25
50	9.03	0.23
60	8.77	0.23
70	8.10	0.21
80	7.54	0.20
90	6.60	0.18
100	5.79	0.16
110	4.96	0.14
120	4.17	0.12
130	3.95	0.11
$k=500$	$\sigma_T=81$	
0.	18.3	0.9
2.2	17.3	0.6
5.	17.2	0.7
7.3	15.8	0.6
10.	14.1	0.5
15.	12.3	0.5
20.	10.7	0.4
30	10.02	0.31
40	9.57	0.25
50	9.14	0.24
60	8.15	0.21
70	7.91	0.20
80	7.23	0.19
90	6.47	0.17
100	5.38	0.15
110	4.65	0.13

θ^*	σ	Δ
$k=500$	$\sigma_T=81$	
120	4.04	0.12
130	3.62	0.10
$k=525$	$\sigma_T=81$	
0.	19.8	0.9
30	10.62	0.33
40	9.63	0.30
50	9.26	0.28
60	8.38	0.22
70	7.96	0.20
80	7.28	0.19
90	6.50	0.17
100	5.52	0.15
110	4.58	0.13
120	3.93	0.11
130	3.46	0.10
$k=550$	$\sigma_T=80$	
0.	18.9	0.6
2.25	18.7	0.6
5.0	18.0	0.6
7.5	16.7	0.5
10.6	15.0	0.5
15.0	12.9	0.4
21.2	10.7	0.3
30	10.35	0.32
40	9.80	0.30
50	9.35	0.28
60	8.63	0.26
70	7.81	0.20
80	7.16	0.18
90	6.10	0.16
100	5.27	0.14
110	4.23	0.11
120	3.54	0.10
130	3.32	0.10
$k=575$	$\sigma_T=83.5$	
0.	19.3	0.9
5.3	18.0	0.6
7.5	15.8	0.5
10.	15.5	0.5
15.	13.6	0.5
20.	11.3	0.4
30	10.84	0.34
40	10.75	0.33
50	10.19	0.31
60	9.21	0.28
70	7.93	0.24
80	7.15	0.18
90	6.45	0.16
100	5.20	0.14
110	4.46	0.12
120	3.77	0.10
130	3.45	0.10
$k=600$	$\sigma_T=83$	
0.	20.6	0.9
2.3	21.	0.9
5.	19.1	0.6
7.6	17.5	0.6
10.6	15.8	0.6
15.1	14.2	0.6
20	11.38	0.35
30	10.13	0.31
40	10.29	0.32
50	10.28	0.30
60	9.82	0.29
70	8.23	0.24

θ^*	σ	Δ
$k=600$	$\sigma_T=83$	
80	7.09	0.18
90	6.21	0.16
100	5.12	0.13
110	4.41	0.12
120	3.67	0.10
130	3.26	0.10
$k=625$	$\sigma_T=86$	
20	11.05	0.34
30	10.59	0.33
40	10.78	0.33
50	10.42	0.31
60	10.41	0.31
70	9.01	0.26
80	7.58	0.22
90	6.22	0.16
100	5.26	0.13
110	4.54	0.12
120	3.75	0.10
130	3.40	0.10
$k=650$	$\sigma_T=91$	
40	11.43	0.35
50	11.15	0.33
60	10.74	0.32
70	9.78	0.29
80	8.44	0.25
90	6.76	0.17
100	5.82	0.15
110	4.66	0.12
120	4.00	0.11
130	3.61	0.10
$k=675$	$\sigma_T=96$	
60	11.39	0.32
70	9.97	0.28
80	9.11	0.26
90	7.66	0.22
100	6.25	0.16
110	5.29	0.13
120	4.53	0.12
130	3.92	0.11
$k=700$	$\sigma_T=102$	
60	11.96	0.34
70	10.65	0.30
80	9.89	0.28
90	8.35	0.24
100	6.71	0.17
110	6.02	0.15
120	5.26	0.14
130	4.66	0.12
$k=725$	$\sigma_T=96$	
70	9.57	0.27
80	9.04	0.26
90	8.39	0.24
100	6.81	0.20
110	6.27	0.16
120	5.49	0.14
130	4.78	0.13
$k=750$	$\sigma_T=86$	
70	8.35	0.24
80	7.70	0.22
90	7.59	0.22
100	6.30	0.18
110	5.60	0.14
120	5.00	0.12
130	4.48	0.12

The reasonably good agreement of the dispersion-theory results extends to rather high energies ($k=500$ MeV). Therefore one can expect that the direct extension of the dispersion isobar model into the region of the second resonance ($k\approx750$ MeV) should yield a reasonable approximation for the background amplitude; i.e., one should expect large changes only in a few physically relevant partial amplitudes, where new resonances occur. A phenomenological fit to the data along these lines has been given in Ref. 3. Some results above $k=500$ MeV are shown in Figs. 10 and 12. The main changes with respect to the first isobar background amplitude appear in the multipoles E_{2-}, M_{2-} of the D_{13} resonance and in the S-wave E_{0+}. There is at the moment a theoretical gap around $k=550$ MeV because of the lack of data at the time the analysis in Ref. 3 was carried out.

TABLE II. Systematic errors.

Source	Error (%)
Bremsstrahlung spectrum	2
Solid angle	2.5
μ-decay contamination	2
Efficiency	1.5
Target absorption	1
Quadratic sum	4.2

B. Near-Forward Direction

Near the forward direction the dispersion-theory results are in excellent agreement with experiments around the first resonance. According to the results in Ref. 3, the discrepancies, which show up at higher energies near the forward direction, can be explained

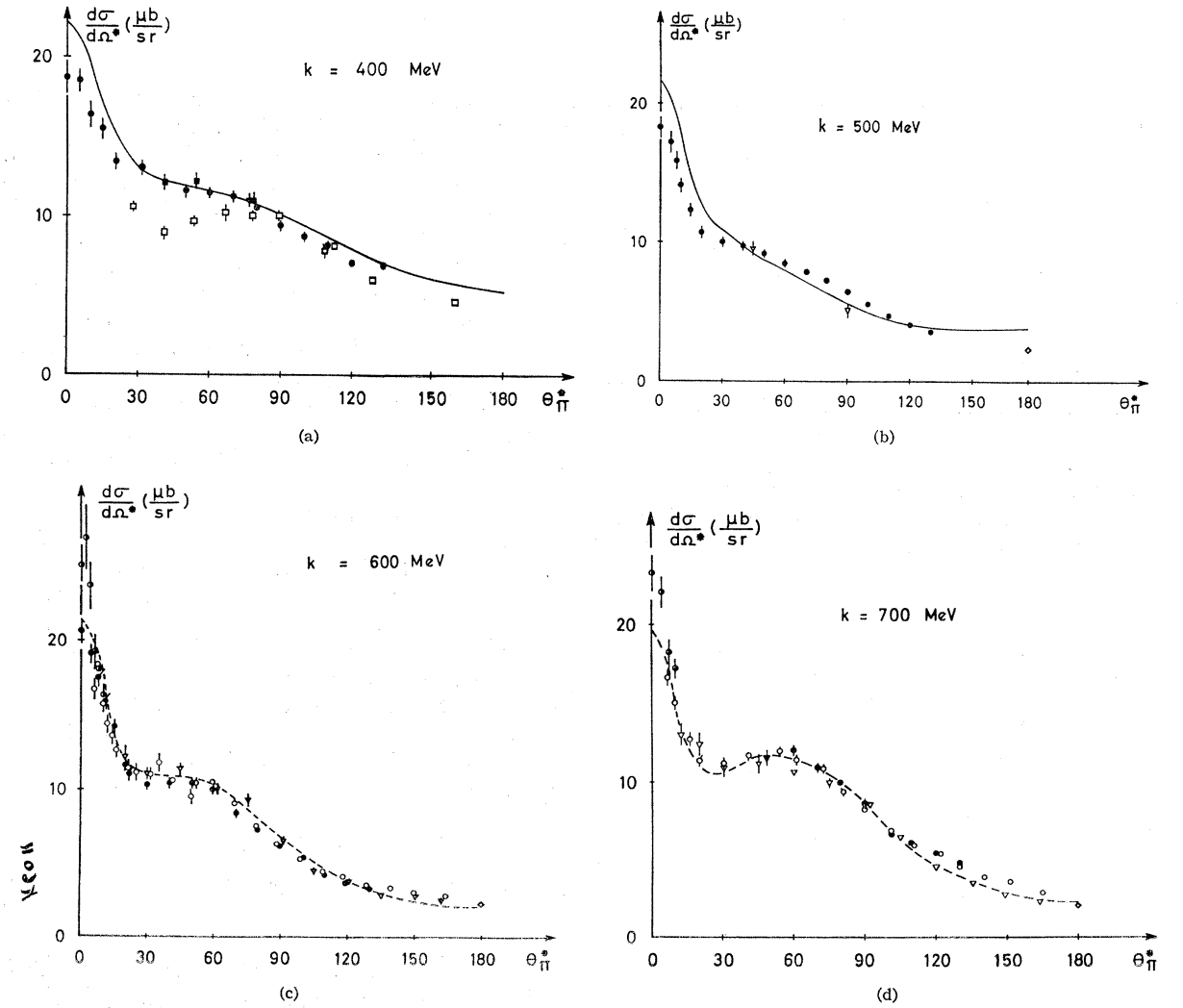

FIG. 10. Angular distribution in the c.m. system. The data points are as follows: ● this experiment; ○ S. D. Ecklund *et al.* (Refs. 1 and 2); ▽ F. D. Dixon *et al.* (Ref. 14); △ A. V. Tollestrup *et al.* (Ref. 7); ▼ M. Heinberg *et al.* (Ref. 8); ▲ R. L. Walker *et al.* (Ref. 9); □ D. Freytag *et al.* (Ref. 15); ■ K. Althoff *et al.* (Ref. 16); ◑ M. Beneventano *et al.* (Ref. 6); ◇ L. Hand and C. Schaerf (Ref. 19 and 20); Solid curve: Ref. 21; dashed curve: Ref. 3.

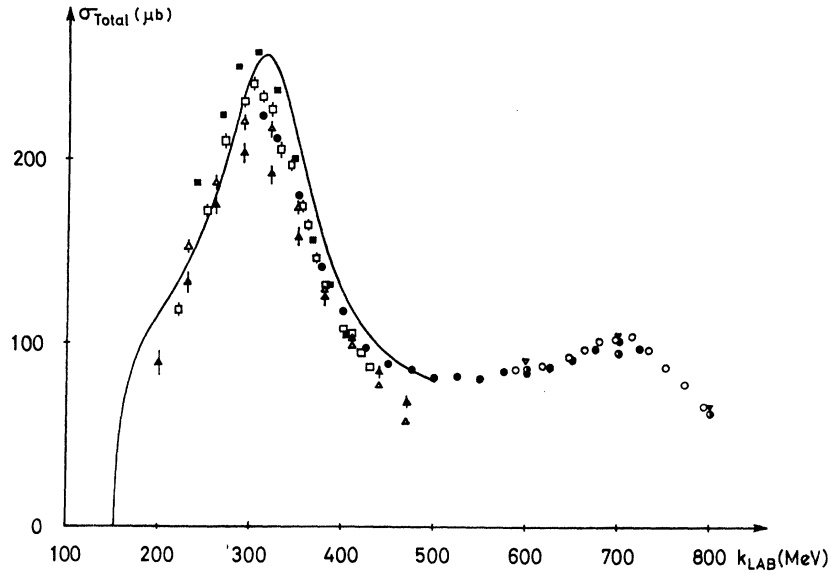

FIG. 11. Total cross sections (μb) as a function of the laboratory photon energy. Solid curve: Ref. 21.

mainly by a small S-wave correction $\Delta\,\mathrm{Re}E_{0+}$, which could arise from unknown high-energy contributions in dispersion integrals. The difference should not be due to the D_{13} resonance because of the ratio

$$E_{2-}/M_{2-}\approx 3 \tag{6}$$

for the contribution of this resonance.[3] With ratio (6) the multipoles E_{2-} and M_{2-} cancel each other in the forward and backward directions.

There is a marked discrepancy near the forward direction between the dispersion-theory calculations in Ref. 21 and Ref. 22. According to Ref. 22, a narrow peak at approximately $\theta^*=10°$ with a dip in forward direction should appear in the energy region considered. Such a behavior of the angular distributions can occur only by differences in very high partial amplitudes. The present data definitely exclude the possibility for such a dip. This is also more compatible with older calculations of Donnachie and Shaw.[25]

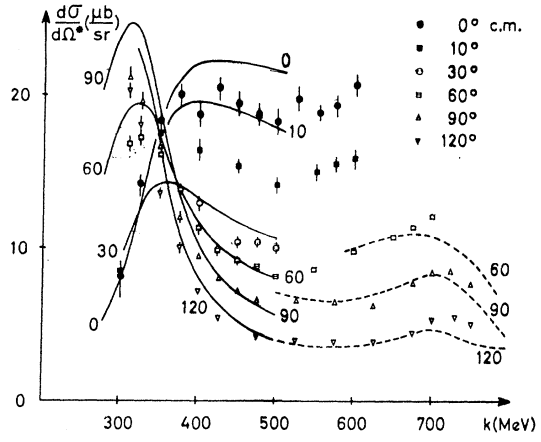

FIG. 12. Excitation curves (θ^* const). Solid curve: Ref. 21; dashed curve: Ref. 3.

According to the phenomenological approach in Ref. 4, the forward peak in the region of the second resonance is explained by the presence of the P_{11}(1466 MeV), S_{11}(1591 MeV), and D_{31}(1635 MeV) resonances. Therefore it is expected in Ref. 4 that at energies above these resonances the forward peak should drop sharply. But by the same argument one might then expect a drop of the forward peak below these resonances. The experimental data and the dispersion-theory results presented here show clearly that the peak in forward direction is already present at lower energies ($k<450$ MeV). Also, at high energies the data of Refs. 1 and 26 do not show the suggested sharp drop of the peak in the forward direction. On the other hand, in the approach of Ref. 3 the forward peak is predominantly an effect which arises by the interference of the pole term with a dispersion-integral contribution produced mainly by the first resonance. In this model no sharp drop of the peak is expected, since the higher resonances give only a small contribution in forward direction. It has been shown in Ref. 27 that with this model the forward peak can be explained up to very high energies $k>1$ GeV. From the point of view of dispersion theory the forward peak in π^+ photoproduction presents no difficulty.

C. P_{11} Resonance (1466 MeV)

Particular care should be taken to look for an influence of the P_{11} resonance on the data around

[25] A. Donnachie and G. Shaw, Ann. Phys. (N. Y.) 37, 333 (1966).
[26] C. Buschhorn, J. Carroll, R. D. Eandi, P. Heide, R. Hübner, W. Kern, U. Kötz, P. Schmüser, and H. J. Skronn, Phys. Rev. Letters 17, 1027 (1966); 18, 571 (1967).
[27] J. Engels, G. Schwiderski, and W. Schmidt, Phys. Rev. 166, 1343 (1968).

$k=670$ MeV. The resonance should directly affect the $J=\frac{1}{2}$ multipole M_{1-}.

An elucidation of the electromagnetic properties of the P_{11} resonance would supply criteria for its classification within symmetry schemes. Lovelace[28] suggested some time ago that the P_{11} resonance should be a member of an SU_3 antidecuplet $\{\bar{1}\bar{0}\}$. In this case one has the very interesting consequence that the electromagnetic excitation of the P_{11} resonance on the proton should be strongly suppressed by U-spin conservation.[29] As a member of the $\{\bar{1}\bar{0}\}$ representation, the P_{11} resonance would belong to U-spin 1 and $\frac{3}{2}$ multiplets. Therefore, the decay of P_{11} into (γ,n) with $U=1$ is allowed but decay into (γ,p) with $U=\frac{1}{2}$ is forbidden. In the conventional description this would be explained as follows. The isovector $M_{1-}{}^{1/2}$ and the isoscalar parts $M_{1-}{}^{0}$, which both lead into final states with isospin $I=\frac{1}{2}$, appear in reactions on the proton and neutron with a different sign:

$$(\gamma,p): \quad M_{1-}{}^{0}+\tfrac{1}{3}M_{1-}{}^{1/2}, \tag{7a}$$

$$(\gamma,n): \quad M_{1-}{}^{0}-\tfrac{1}{3}M_{1-}{}^{1/2}. \tag{7b}$$

Therefore, if

$$M_{1-}{}^{0}\approx\mp\tfrac{1}{3}M_{1-}{}^{1/2}, \tag{8}$$

there will be an enhancement in the one case and a cancellation in the other. Relation (8) with the upper sign is approximately valid in the isobar approximation.[3,21] On the basis of the very scanty data on π^+, π^- photoproduction it is expected[3] that relation (8) with the upper sign is satisfied by the contribution of the P_{11} resonance. For a more detailed discussion see Refs. 3 and 30.

Now, the π^+-excitation curves (Fig. 12) from the present data and the total cross section (Fig. 11) indeed do not reveal any obvious structure around $k=670$ MeV that could unambiguously indicate the excitation of this resonance on the proton. One observes only a smooth increase of the cross section in this energy region, which should be mostly due to the tail of the strong D_{13} resonance. From visual inspection of the systematic measurements in this energy region one can only conclude (a) that the excitation of the P_{11} resonance in π^+ photoproduction is either weak, or (b) it is strong but cannot be detected visually because of its large width, low J value and the high inelasticity. It could happen that this resonance can only be distinguished from the smooth background amplitude by using detailed models or partial-amplitude analyses.[3,4] In pion-nucleon scattering one is often confronted with such a situation.[31]

In π^+ and π^0 photoproduction on the proton the same isospin combination of multipoles appears, which lead into the isospin $I=\frac{1}{2}$, P_{11} final state

$$M_{1-}{}^{\pi+}=\sqrt{2}(M_{1-}{}^{0}+\tfrac{1}{3}M_{1-}{}^{1/2}-\tfrac{1}{3}M_{1-}{}^{3/2}), \tag{9a}$$

$$M_{1-}{}^{\pi^0}=M_{1-}{}^{0}+\tfrac{1}{3}M_{1-}{}^{1/2}+\tfrac{2}{3}M_{1-}{}^{3/2}. \tag{9b}$$

Therefore in π^0 photoproduction the situation with respect to the P_{11} resonance should be similar.

Contrary to the phenomenological approach in Ref. 3, one has to conclude from the results in Ref. 4 that the electromagnetic excitation of the P_{11} resonance on the proton is strong. In both works[3,4] a partial-amplitude analysis was tried (in a restricted sense) by different methods, but without the benefit of present data.

In Ref. 3 an approximate background amplitude, which is derived from the P_{33}-isobar approximation, is used as input. Thus it is possible to restrict from the very beginning the high ambiguity which one encounters in this kind of work. A fit to the data is then obtained by adjusting the physical relevant partial amplitudes individually. In Ref. 4 the fullest possible use of the known pion-nucleon scattering phase shifts is made by using an isobar model for the resonances and imposing the Watson theorem on the elastic partial amplitudes. The free parameters are then fitted to the available data. Especially in π^0 photoproduction all the details of the data are not fully understood as a result of insufficient experimental and theoretical information.

In all processes considered, both methods yield completely different results for the $J=\frac{1}{2}$ multipoles E_{0+} and M_{1-}. This may explain the different conclusion with respect to the role of the P_{11} resonance. Of course, the results for the $J=\frac{1}{2}$ multipoles are particularly ambiguous, since these multipoles determine mainly the slowly varying background, which is usually not uniquely fixed because of systematic errors between different experiments.

However, at present it seems very unlikely that unknown high-energy contributions in the dispersion integrals for the $J=\frac{1}{2}$ multipoles E_{0+} and M_{1-} can produce a rapid change with energy between $k=500$ and 600 MeV for *both* multipoles and thereby reconcile the results of Ref. 4 with the isobar approximation[21,22] at lower energies. Furthermore, the energy variation of E_{0+} and M_{1-} is also restricted by the smooth behavior of the forward peak (see Sec. VII B). So at present it is more likely that the electromagnetic excitation of the P_{11} resonance on the proton is forbidden, as suggested by the results in Ref. 3 and by naive visual analysis of the present data.

---

[28] C. Lovelace, CERN Report No. 65/1674/5-TH. 628, 1965 (unpublished).
[29] H. J. Lipkin, Phys. Letters **12**, 154 (1964).
[30] A. Donnachie, Phys. Letters **24B**, 420 (1967).
[31] A. Donnachie, R. G. Kirsopp, and C. Lovelace, CERN Report No. 67/1283/5-TH. 838, Geneva, 1967 (unpublished).

ACKNOWLEDGMENTS

Our thanks go to Professor A. Blanc-Lapierre for extending to us the facilities of the Orsay Laboratory. We wish to thank G. Brochard and F. Richard for assistance in data taking, G. Bouvard and G. Lissilour for help in the installation of the experiment. Two of us (C.B. and J.P-Y-J) are grateful to Dr. Nguyen Ngoc for assistance in the design and test of the Čerenkov counter. We are grateful for the help provided by the technological group directed by V. Round and by the accelerator team directed by Dr. Burnod and Dr. Milman.

PHYSICAL REVIEW VOLUME 172, NUMBER 5 25 AUGUST 1968

Strange-Particle Production in 8-BeV/c Proton-Proton Interactions*†

M. FIREBAUGH,‡ G. ASCOLI, E. L. GOLDWASSER, R. D. SARD, AND J. WRAY
Department of Physics, University of Illinois, Urbana, Illinois
(Received 18 December 1967)

A systematic survey of strange-particle final states produced by 8-BeV/c protons was made in the BNL 80-in. hydrogen bubble chamber. Cross sections were measured for some 33 reactions. The ratio of the cross section for the $K\bar{K}$ channels to the total strange-particle cross section was measured to be 0.12 and appears to be rising in this momentum region. The total cross section for strange-particle production is estimated as 1.8±0.2 mb. Comparison is made of the data with the predictions of the one-pion-exchange model, and at least partial agreement occurs for the $K^+p\Lambda$ and $\pi KN\Sigma$ final states. The $Kp\Sigma$ states appear to contain $N^*(1924)\to K\Sigma$, and the $\pi KN\Lambda$ states all include $Y^*(1385)$ production with the $\pi^+K^0p\Lambda$ state also containing $N^*(1236)$ and $K^*(890)$ production. An examination of the five- and six-body K,Λ states indicates strong $Y^*(1385)$ and $N^*(1236)$ production. Finally, all final states containing a K and a Λ show a dependence on $M(K,\Lambda)$ which is well parametrized by a Breit-Wigner shape with $M_0=1777$ MeV and $\Gamma=345$ MeV. This behavior is interpreted as being consistent with one-pion exchange as the dominant mechanism for these reactions.

I. INTRODUCTION

PREVIOUS experiments on strange particles produced in p-p interactions have been reported at lower momenta (up to 6.6 BeV/c)[1] and certain topologies of strange-particle events have been examined at higher momenta (10 and 24.5 BeV/c).[2] The present experiment was initiated for several reasons: to test the extent to which one-pion exchange (OPE) contributes in this unexplored momentum region, to examine the 2-baryon mass spectra for possible $B=2, S=-1$ resonances,[3] and to determine the amount of production of the well-known resonances. The data for the experiment consisted of about 37 000 pictures of the Brookhaven 80-in. hydrogen bubble chamber exposed to 7.87 BeV/c protons at the AGS.[4]

II. ANALYSIS PROCEDURE

A. Scanning and Measuring

The entire film was scanned once in all three views and a second time in either two or three views. The events of interest were 2-, 4-, or 6-prong interactions with one or more associated kinks or V's. When such

* Work supported in part by the U. S. Atomic Energy Commission.

† Portions of this work were presented by M. Firebaugh as a thesis to the Department of Physics of the University of Illinois in partial fulfillment of the requirements for the Ph.D. degree.

‡ Present address: Department of Physics, University of Wisconsin, Madison, Wisc.

[1] Previous $p+p\to$ (strange particle) experiments at momenta <8 BeV/c: 3.68 BeV/c, R. I. Louttit, T. W. Morris, D. C. Rahm, R. R. Rau, A. M. Thorndike, and W. J. Willis, Phys. Rev. **123**, 1465 (1961); 5.0 BeV/c, E. Bierman, A. P. Colleraine, and U. Nauenberg, *ibid.* **147**, 922 (1966); 5.5 BeV/c, G. Alexander, O. Benary, N. Kidron, A. Shapira, R. Yaari, and G. Yekutieli, Phys. Rev. Letters **13**, 355A (1964); 5.4 and 6.6 BeV/c, William Dunwoodie, William E. Slater, Harold K. Ticho, Gerald A. Smith, Arthur B. Wicklund, and Stanley G. Wojcicki (unpublished); 6.0 BeV/c, W. Chinowsky, R. R. Kinsey, S. L. Klein, M. Mandelkern, J. Schultz, F. Martin, M. L. Perl, and T. H. Tan, Phys. Rev. **165**, 1466 (1968); A. B. Wicklund, G. A. Smith, W. Woischnig, S. Wojcicki, Bull. Am. Phys. Soc. **12**, 505 (1967); G. A. Smith, A. B. Wicklund, S. Wojcicki, *ibid.* **12**, 505 (1967).

[2] Previous $p+p\to$ (strange particle) experiments at moments >8 BeV/c: 10.0 BeV/c, S. O. Holmgren, S. Nilsson, T. Olhede, and N. Yamdagni, Nuovo Cimento **51**, 305 (1967); 24.5 BeV/c, J. Bartke, W. A. Cooper, B. Czapp, H. Filthuth, Y. Goldschmidt-Clermont, L. Montanet, D. R. O. Morrison, S. Nilsson, Ch. Peyrou, R. Sosnowki, A. Bigi, R. Carrara, C. Fransinetti, and I. Mannelli, *ibid.* **29**, 8 (1963); A. De Marco-Trabucco, L. Montanet, S. Nilsson, Nucl. Phys. **60**, 209 (1964).

[3] Experiments reporting possible ΛN mass enhancements at the following mass values: 2059 MeV, A. C. Melissinos, N. W. Reay, J. T. Reed, T. Yamanouchi, E. Sacharidis, S. J. Lindenbaum, S. Ozaki, and L. C. L. Yuan, Phys. Rev. Letters **14**, 604 (1965); 2098 MeV, H. O. Chon, K. H. Bhatt, and W. M. Bugg, *ibid.* **13**, 668 (1964); 2115 MeV, M. Meer, J. Mueller, M. Schneeberger, S. E. Wolf, J. Albright, E. B. Brucher, J. Lannutti, J. O'Neall, and W. H. Sims, Bull. Am. Phys. Soc. **11**, 342 (1966); 2220 MeV, T. Buran, O. Eivindson, O. Skjeffestad, H. Tofte, and I. Vegge, Phys. Letters **20**, 318 (1966); 2360 MeV, P. A. Piroue, *ibid.* **11**, 164 (1964).

[4] I. Skillicorn and M. S. Webster, BNL Bubble Chamber Report No. H10, 1962 (unpublished).